Biomedical Signal Processing and Control 87 (2024) 105512

Contents lists available at ScienceDirect

Biomedical Signal Processing and Control

journal homepage: www.elsevier.com/locate/bspc

Unveiling the alterations in the frequency-dependent connectivity structure of MEG signals in mild cognitive impairment and Alzheimer's disease

Víctor Rodríguez-González [a,b,*], Pablo Núñez [a,b,c], Carlos Gómez [a,b], Hideyuki Hoshi [d], Yoshihito Shigihara [d], Roberto Hornero [a,b,e], Jesús Poza [a,b,e]

[a] Biomedical Engineering Group, University of Valladolid, Valladolid, Spain
[b] Centro de Investigación Biomédica en Red de Bioingeniería, Biomateriales y Nanomedicina, Instituto de Salud Carlos III (CIBER-BBN), Spain
[c] Coma Science Group, GIGA-Consciousness, University of Liège, Liège, Belgium
[d] Hokuto Hospital, Obihiro, Japan
[e] IMUVA, Instituto de Investigación en Matemáticas, University of Valladolid, Valladolid, Spain

ARTICLE INFO

Keywords:
Connectivity-based Meta-Bands (CMB)
Meta-Bands
Connectivity
Alzheimer's disease (AD)
Mild cognitive impairment (MCI)

ABSTRACT

Mild cognitive impairment (MCI) and dementia due to Alzheimer's disease (AD) are neurological disorders that affect cognition, brain function, and memory. Magnetoencephalography (MEG) is a neuroimaging technique used to study changes in brain oscillations caused by neural pathologies. However, MEG studies often use fixed frequency bands, assuming a common frequency structure and overlooking both subject-specific variations and the potential influence of pathologies on frequency distribution. To address this issue, a novel methodology called Connectivity-based Meta-Bands (CMB) was applied to obtain a subject-specific functional connectivity-based frequency bands segmentation. Resting-state MEG activity was acquired from 161 participants: 67 healthy controls, 44 MCI patients, and 50 AD patients. The CMB algorithm was used to identify "meta-bands" (*i.e.*, recurrent network topologies across frequencies). The meta-bands were used to extract an individualised frequency band segmentation. The network topology of the meta-bands and their sequencing were analysed to identify alterations associated with MCI and AD in the underlying frequency-dependent connectivity structure. We found that MCI and AD alter the neural network topology, leading to connectivity patterns both more widespread in the frequency spectrum and heterogeneous. Furthermore, the meta-band frequency sequencing was modified, with MCI and AD patients exhibiting sequences with increased complexity, suggesting a progressive dilution of the frequency structure. The study highlights the relevance of considering the impact of neural pathologies on the frequency-dependent connectivity structure and the potential bias introduced by using fixed frequency bands in MEG studies.

1. Introduction

Alzheimer's disease (AD) is a serious clinical and social challenge, particularly in developed nations [1]. AD is characterised by progressive neuronal damage that results in cell death. This pathology is the leading cause of dementia, and affects the behaviour, cognition, memory, and functional ability of the patients [1]. Mild cognitive impairment (MCI) is typically regarded as the prodromal phase of AD, in which patients experience symptoms that are not compatible with healthy ageing but are not severe enough to warrant a diagnosis of dementia [1]. Moreover, the prevalence of individuals with AD or MCI is expected to continue growing; therefore, AD is deemed one of the most important challenges that healthcare systems will face in the coming years [1].

Neuroimaging techniques are powerful tools to study brain activity. Specifically, neurophysiological techniques such as electroencephalography (EEG) and magnetoencephalography (MEG) offer several advantages compared to other techniques such as Positron Emission Tomography (PET) or functional Magnetic Resonance Imaging (fMRI), due to their non-invasiveness (compared with PET) and ability to provide high temporal resolution (compared with both) [2]. This latter property allows to capture the entire range of brain variability, from the slower waves to the faster oscillations. This feature is of great importance, given that it has been suggested that neural variability may play an important role in higher cognitive functions [3,4]. This study is

* Corresponding author at: Biomedical Engineering Group, University of Valladolid, Valladolid, Spain.
E-mail addresses: victor.rodriguez@uva.es (V. Rodríguez-González), jesus.poza@uva.es (J. Poza).

https://doi.org/10.1016/j.bspc.2023.105512
Received 7 May 2023; Received in revised form 20 September 2023; Accepted 24 September 2023
Available online 30 September 2023

focused on MEG, as it provides higher spatial resolution and improved robustness against noise and volume conduction than EEG [5–8].

The neurophysiological dynamics recorded by MEG can be altered by diverse diseases that affect the central nervous system. A more profound understanding of their pathological fingerprint can be achieved by studying these alterations. Previous research has investigated the changes in MEG activity caused by MCI and AD [9–11]. Some of these changes can be observed through local activation analyses, *i.e.*, when studying the time courses of the neural signal at sensors or sources individually [9,12,13]. These local activation measures have revealed that MCI and AD lead to slower brain oscillations with reduced irregularity, complexity, and variability [14–16]. Furthermore, it has been shown that both MCI and AD impact static functional connectivity, and are considered as "disconnection syndromes" [9–11,17–19]. In recent years, there has been a growing interest in investigating how MCI and AD affect dynamic functional connectivity patterns (dFC) [20–23]. This approach is grounded on the premise that the interactions between brain regions do not remain stable across time [22,24]. Some intriguing discoveries have emerged in this field, such as aberrant dFC patterns in resting-state, which have been linked to MCI and AD. However, many of these studies consider that neural activity can be grouped in fixed frequency ranges, as they are conducted after filtering the signals in the so-called "canonical" frequency bands.

Although the canonical frequency bands are supported by a large array of literature, they have some limitations, including: Rodríguez-González et al. [8] and Newson and Thiagarajan [25]: (i) they were established around eight decades ago when the acquisition technology differed significantly from modern systems; (ii) the modern analysis algorithms have considerably evolved since the original definition of the canonical frequency bands; (iii) the frequency boundaries are not consistent across studies, thereby hindering the replication of findings; and (iv) the bands are fixed and, thus, they do not account for subject-specific neural oscillatory patterns. In a previous study, we found that, these bands accurately reflect the group-level activity in MEG signals, however, they overlook important information about subject-specific neural idiosyncrasies [8].

Previous research has demonstrated that MCI and AD alter the time-dependent connectivity structure, leading to less stable brain states in time [21]. There, Núñez and colleagues employed the canonical frequency bands, considering the frequency patterns comparable for controls, MCI, and AD patients. However, in this study employed the novel Connectivity-based Meta-Bands (CMB) methodology introduced in [8] to evaluate whether these pathologies (MCI and AD) are affecting the frequency-dependent connectivity structure of neural activity, in addition to the time-dependent connectivity structure, as Núñez and colleagues demonstrated [21,22,26]. To the best of our knowledge, this is the first time that the influence of MCI and AD in this network-based frequency structure is assessed. We hypothesised that MCI and AD disrupt the meta-band structure, that is, the neural mechanisms that regulate the frequency-dependent connectivity structure. Therefore, two main objectives were proposed for the present study: (i) to evaluate the sensitivity of the CMB algorithm to the alterations elicited by MCI and AD; and (ii) to develop new metrics to characterise these changes.

2. Materials and methodology

2.1. Participants

A total of 161 participants were included in the study: 67 healthy elderly controls, 44 patients with MCI, and 50 patients with dementia due to AD. The diagnoses were carried out according to the National Institute on Aging and Alzheimer's Association (NIA-AA) criteria [27,28]. The healthy elderly controls (HC) did not suffer psychiatric disorders nor have a history of neurological alterations.

Statistical tests were conducted to evaluate differences between sociodemographic variables. The groups displayed differences in age (χ^2 = 44.48, p-value < 0.001, Kruskal–Wallis test), but not in sex (χ^2 = 5.16, p-value = 0.076, Chi-squared test). The sociodemographic and clinical data of the sample are displayed in Table 1.

Table 1
Sociodemographic and clinical data of the participants. HC: cognitively healthy elderly controls; MCI: patients with mild cognitive impairment; AD: patients with dementia due to Alzheimer's disease; m: mean; std: standard deviation; M: male; F: female; MMSE: Mini-mental state examination.

Feature	Group		
	HC	MCI	AD
Number of subjects	67	44	50
Age (years, m ± std)	71.0 ± 7.6	77.2 ± 6.1	81.6 ± 7.0
Sex (M:F)	32:35	12:32	23:27
MMSE (m ± std)	29.5 ± 0.8	26.0 ± 2.6	17.4 ± 5.7

Participants and caregivers provided their written informed consent for the study before their participation. All the analyses were conducted in accordance to the Code of Ethics of the World Medical Association (Declaration of Helsinki). The Ethics Committees of Hokuto Hospital (Obihiro, Japan; approval numbers: #1001, #1007-R3, #1020, and #1038), and Kumagaya General Hospital (Kumagaya, Japan; approval numbers: #25, #26, #51, and #76) gave their approval for the research protocol.

2.2. MEG recordings

Magnetoencephalographic (MEG) resting-state neural activity was acquired for 5 min for each subject. During the recording, participants remained in supine position and awake, with their eyes closed. All the recordings were monitored in real time by the researchers in order to ensure safety and prevent somnolence.

The MEG acquisition took place in the Hokuto Hospital and Kumagaya General Hospital using a MEG Vision PQ1160C (Yokogawa Electric, sampling frequency of 1000 Hz) and a RICOH160-1 (RICOH Company, f_s = 2000 Hz), respectively. Both systems are functionally equivalent, consisting on a whole-head 160-channel axial gradiometers system placed in a magnetically-shielded room. Before the recordings, the head position was scanned by means of coil markers placed on the head of the patient.

2.2.1. MEG preprocessing

The MEG recordings obtained at Kumagaya General Hospital were downsampled to 1000 Hz to homogenise the MEG recordings. Then, the same 5-step preprocessing protocol was applied to all the signals [29]: (i) application of the SOurce-estimate-Utilising Noise-Discarding (SOUND) algorithm to remove artifacts [30]; (ii) finite impulse response (FIR) bandpass filtering between 1 and 70 Hz to limit noise bandwidth; (iii) finite impulse response (FIR) bandstop filtering between 49 and 51 Hz to remove powerline interference; (iv) artifact rejection by means of independent component analysis (ICA); and (v) selection of 5-s artifact-free trials by visual inspection.

2.2.2. Source inversion

Source-level time courses were obtained by means of the weighted minimum norm estimation (wMNE) method [31]. This method restricts the solutions by minimising the energy of the solution, weighting deeper sources to ease their detection [31]. This algorithm displays good performance with MEG signals [31–34]. The implementation of this method is freely available in the Brainstorm toolbox (http://neuroimage.usc.edu/brainstorm) [35]. The ICBM152 anatomical template was used to create the forward model [36,37]. A boundary element method head model with three layers (brain, skull, and scalp) was created by means of OpenMEEG [29,38]. Source space was restricted to the cortex, considering 15 000 sources, which were limited to be normal to cortex [29]. Sources in opposite directions were flipped to avoid having neighbouring generators blurring the sources [39]. Finally, the 15 000 sources were grouped in the 68 regions of interest (ROIs) provided by the Desikan-Killiany atlas [29,40,41].

2.3. Methods: Connectivity-based meta-bands

Our analyses were based on a novel methodology developed for extracting the meta-bands (*i.e.*, network topologies repeated across frequencies, that are considered as attractors of the connectivity topology in each frequency bin): the CMB algorithm [8]. These meta-bands are frequency ranges defined on the basis of the similarity of their underlying connectivity patterns [8]. In this study, the original processing pipeline was adapted to ease the characterisation of the pathological alterations, and reduce its computational burden, considering a potential clinical implementation. The CMB algorithm provides a thorough description of the connectivity patterns with a high frequency resolution. Then, these frequency-dependent connectivity patterns are grouped in communities (*i.e.*, meta-bands) by means of the Louvain GJA algorithm. Please refer to Rodríguez-González et al. [8] for a full description of the algorithm.

The same hyper-parameters as in [8] were employed, since they have been optimised for MEG signals with similar characteristics to those used here: a sampling frequency of 1000 Hz, filter bandwidth of 1 Hz, frequency overlapping of the filters of 50%, and filter order of 500. Additionally, the analyses were conducted in the frequency range between 1 and 70 Hz, discarding the connectivity matrices between 47.5 and 52.5 Hz to avoid the influence of powerline interference and the filtering process associated to it [8,42].

Firstly, MEG signals were preprocessed and their source-level time courses were extracted by means of the wMNE algorithm, as described in Section 2.2.2. Of note, the algorithm hyperparameters (*i.e.*, filter order, frequency resolution, and filter overlap) were set according to the values established in [8]. Then, based on the hyper-parameters previously defined, a narrowband 1-Hz filter bank was applied to the MEG recordings at source level. Next, the functional connectivity was estimated for each of these narrowband signals using the orthogonalised version of the amplitude envelope correlation (AEC). The HC sample was randomly divided into two different subsets: (i) the HC_{train} subset, composed of 37 subjects; and (ii) the HC_{test} subset, composed of 30 subjects. With this, we pretended to emulate a real clinical environment. There, when the diagnostic support tool is developed, the "reference" meta-band topology and sequencing (*i.e.*, those for cognitively healthy controls) are extracted only once at the beginning and maintained throughout all the study (*i.e.*, they should not change with every inclusion of a new subject). Furthermore, this division also supports the robustness of the methodology, as it can be observed that the data distribution for the HC_{test} group is closer to the HC_{train} than the other groups (MCI and AD). After that, frequency-dependent recurrence plots (RPs) were created for the HC_{train} subset, and the connectivity community detection was carried out by means of the Louvain GJA algorithm. Following this process, we obtained the frequency activation sequence (FAS), as well as the meta-band network topologies for the HC_{train} group. Of note, the meta-bands were ordered according to their frequency of occurrence (*i.e.*, the first meta-bands will be the one that is active in the largest number of bins in the FAS). Next, these meta-band network topologies were used as reference to compare with the frequency-dependent connectivity matrices associated to the other groups (HC_{test} subset, MCI patients, and AD patients) and to generate the corresponding FAS. Further details of the methodology are provided in the Supplementary Material.

The meta-bands obtained for the HC_{train} sample were used as the canonical connectivity patterns of a "healthy" brain. This method facilitates direct comparisons, not only of the meta-band structure itself, but also of the activation sequence across frequencies. Otherwise, as the meta-bands can be different across groups, their comparison would not be straightforward. Therefore, this approach allows for implementation in clinical settings, as it is scalable and can easily accommodate new pathological groups without requiring re-computation of the meta-bands for each group every time a new patient is included [8]. In addition, the definition of a HC_{test} sample avoids the bias of estimating the parameters with the same subjects employed to extract the meta-band topologies.

The community detection step returns two main results: (i) the network topology associated to each of the meta-bands and (ii) the FAS. The former describes the average connectivity matrix for each meta-band, which groups the recurrent network topologies across frequencies. On the other hand, the FAS is a categorical function specifying the dominant meta-band in each frequency bin, *i.e.*, the meta-band network topology displaying highest correlation with each frequency-specific connectivity matrix.

The network topologies of the meta-bands previously obtained were used to generate the FAS for the other groups (HC_{test}, MCI patients, and AD patients) by correlating those topologies with the connectivity matrices of each frequency bin. The meta-bands for the other groups were not extracted, as the objective of the present study was to assess the deviation that AD and MCI provokes regarding the meta-bands (and its associated FAS) from a healthy elderly population. A summary of this methodology is graphically represented in Fig. 1.

2.4. Novel metrics to parametrise the frequency activation sequence (FAS)

In order to parametrise the frequency structure of the meta-bands, we used a diverse array of metrics, some of them defined for the first time in the context of the present work. These metrics can be grouped in two categories, depending on the characteristics of the frequency-dependent connectivity structure they measure: (i) alterations in the frequency-dependent connectivity topology, quantified using the Attraction Strength (AS), Degree of Dominance (DoD), and Topological Adaptation (TA); and (ii) alterations in the meta-band sequencing, summarised by means of the Switching Rate (SR), and Band Complexity (B_{LZC}). While AS and DoD were already presented in [8], TA, SR and B_{LZC} are introduced here for the first time.

2.4.1. Topological adaptation

The Topological Adaptation (TA) summarises the similarity of the frequency-dependent connectivity matrices assigned to a given meta-band and the reference topology of each meta-band obtained from the HC_{train} group. It is estimated as the global Spearman correlation between the mean of all the connectivity matrices assigned to a specific meta-band, and the topology of a specific meta-band. It is computed as follows:

$$TA_i = \mathrm{corr}\left(m_i, M_i\right), \tag{1}$$

where m_i is the mean of all the connectivity matrices assigned to the meta-band i, and M_i is the connectivity matrix associated to the meta-band i. The higher the values of TA, the better adaptation of the frequency-dependent connectivity matrices to the extracted meta-bands.

2.4.2. Attraction Strength

The Attraction Strength (AS) measures the degree of adaptation of the functional connectivity matrix in each frequency bin to its corresponding meta-band [8]. It is formally defined as the Spearman correlation between each frequency-dependent connectivity matrix and the corresponding meta-band [8].

$$AS(i) = corr(a_i, M_{di}), \tag{2}$$

where $corr(\cdot)$ is the Spearman correlation, a_i the connectivity matrix at the frequency i, and M_{di} the network topology of the dominant meta-band at the frequency i. Higher values mean better fit to the corresponding dominant meta-band.

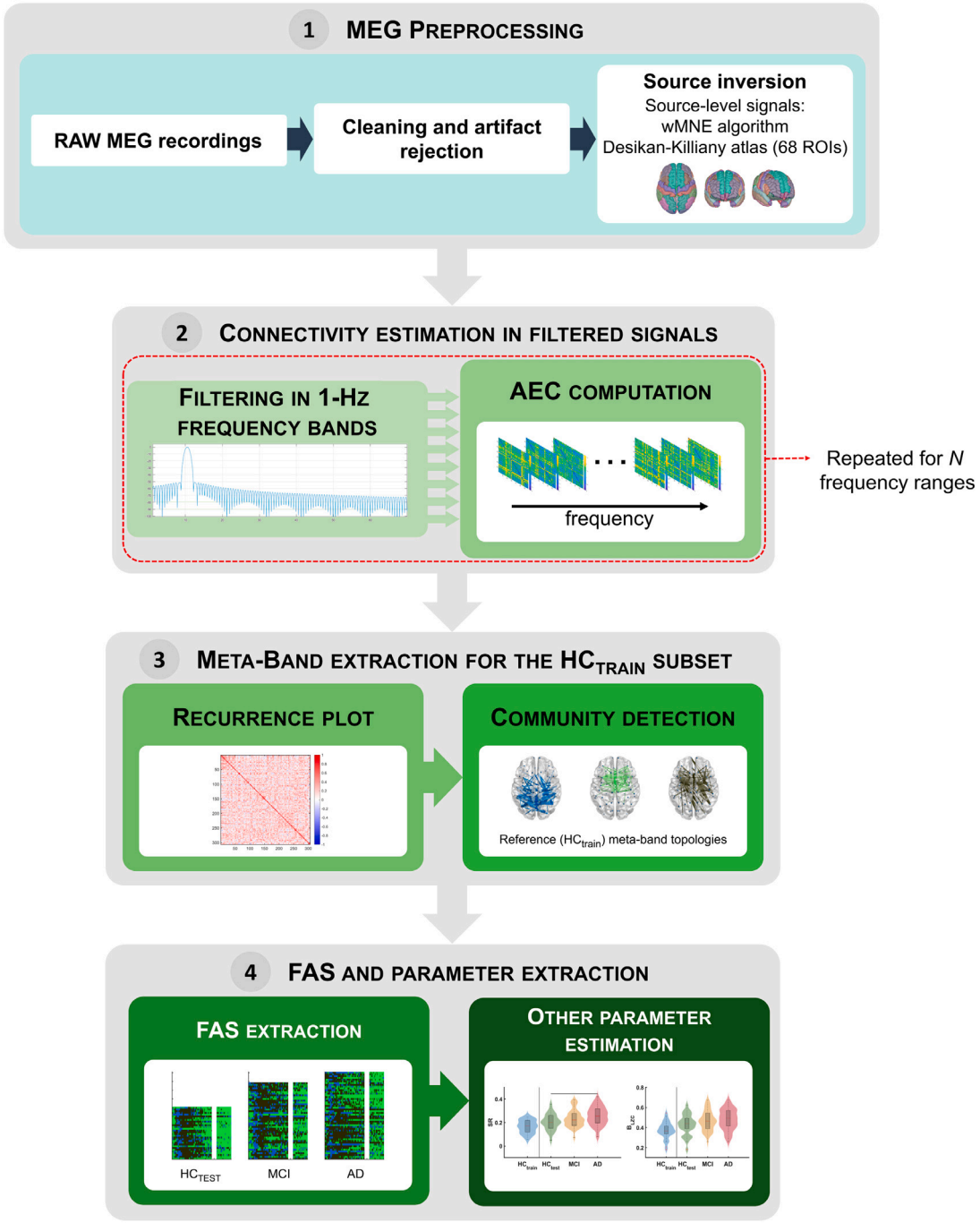

Fig. 1. Flow diagram of the employed methodology to assess the frequency-dependent connectivity structure of MEG activity: (1) Preprocessing — The signals are preprocessed, and their source-level time courses reconstructed; (2) Connectivity estimation in band-limited signals — For all the subjects, MEG signals are filtered using a narrowband 1-Hz filter bank, and the orthogonalised version of the amplitude envelope correlation (AEC) is used to estimate the functional connectivity for each filtered signal; (3) Meta-band extraction for the HC_{train} subset — For a subset of the healthy controls sample (the ones considered for training), recurrence plots describing repetitions of the frequency-dependent connectivity structure are computed, and a community detection process is carried out based on the Louvain GJA algorithm; (4) Extraction of the frequency activation sequence (FAS) and other parameters for the other groups — Using the meta-bands extracted in step (3), the FAS, Topological Adaptation (TA), Attraction Strength (AS), Degree of Dominance (DoD), Switching Rate (SR), and Band Complexity (B_{LZC}) are obtained for the other groups under study (HC_{test} subset, MCI patients, and AD patients).

2.4.3. Degree of Dominance

The Degree of Dominance (DoD) evaluates how each connectivity matrix in a given frequency bin fits its corresponding dominant meta-band as opposed to the non-dominant meta-bands [8]. It is computed as the AS minus the average Spearman correlation between the connectivity matrix in each frequency bin and the corresponding non-dominant meta-bands [8]:

$$DoD(i) = corr(a_i, M_{di}) - \frac{1}{m-1}\sum_{\substack{n=1 \\ n\neq d}}^{m} corr(a_i, M_{ni}), \tag{3}$$

where M_{ni} is the network topology of each of the non-dominant meta-bands at the frequency i, and m the number of meta-bands identified

with the HC_{train} subset. Higher values mean better fit to the dominant meta-band when compared with the non-dominant meta-bands.

2.4.4. Switching rate

The switching Rate (SR) parameter measures the proportion of frequency bins where a meta-band change occurs as a fraction of the total number of frequency bins. Higher values of SR indicate less stable meta-bands.

2.4.5. Band complexity

The Band Complexity (B_{LZC}) is defined as the Lempel–Ziv Complexity of the FAS. Further details on the computation of the Lempel–Ziv Complexity can be found in [43]. Higher values are associated with an increased complexity in the FAS structure, which is related to a higher number of different meta-band sequences. Similar metrics have been used to characterise the complexity of the activation of time meta-states [22,24].

SR and B_{LZC} provide complementary information. The former computes only the number of meta-band changes, while the latter calculates the complexity of the meta-band sequencing. For example, a subject continuously changing between meta-band 1 and 2 will display high SR values, but low B_{LZC} ones.

2.5. Statistical analyses

To evaluate the between-group statistically significant differences in the parameters, a bootstrapping approach was employed [44,45]. The distribution of the average differences between all pairs of groups was computed after bootstrapping (resampling with replacement) the groups 50 000 times for each comparison [44,45]. The p-value was considered as twice the proportion of average differences greater or less than 0 (the smallest of them) [44,45]. For each comparison, it was reported the grand-average of the difference values and the p-value [45]. The multiple comparison problem was controlled by applying false discovery rate (FDR) correction using the Benjamini and Hochberg procedure [45,46].

3. Results

3.1. Potential impact of age as confounding factor

To prevent misinterpretation of results, the impact of age as confounding factor was evaluated in the parameters under study. Results showed no significant impact in any of the parameters under study (p-value > 0.05, Spearman's correlation test, FDR corrected).

3.2. Computation of the frequency activation sequencing (FAS)

The network topologies of the three main meta-bands detected for the HC_{train} subset, as well as the corresponding FAS are depicted in Fig. 2. The FAS for the HC_{test} subset, MCI patients, and AD patients groups are also included in Fig. 2. There, it can be appreciated that the advance of the pathology progressively blurs the underlying frequency-dependent connectivity structure.

For the HC_{train} subset, three main meta bands were identified: meta-band 1, with a widespread network topology for low (around the delta band) and high frequencies (around gamma band); meta-band 2, around beta frequencies with a mid-frontal topology; and meta-band 3, with a posterior distribution of connections around alpha and very few frequency bins around high beta. The FAS for the HC_{test} subset displays a similar pattern to that for the HC_{train} subset. On the other hand, it can be observed that the FAS for the MCI and AD patients groups revealed a gradual degradation on the frequency-dependent connectivity structure: the meta-bands 2 and 3 are altered, progressively losing stability and presence.

Also, it is noteworthy that the values for the HC_{train} are closer to the HC_{test} than to the other groups. This happens consistently for all the metrics that will be further evaluated in this manuscript, and it is very relevant as it points out that both HC groups show coherent behaviour.

3.3. Alterations in the structure of the frequency-dependent connectivity

The TA values for the different combinations of connectivity matrices and meta-bands are depicted in Fig. 3. This metric evaluates the alterations that the pathology elicits in the meta-band topological structure. The panel in row i and column j represents the TA of the mean of the connectivity matrices assigned to meta-band i and the network topology of meta-band j. For all the comparisons, a similar tendency arises, with lower values as dementia progresses. For all the comparisons, statistically significant differences between HC and AD patients can be observed. Furthermore, all the comparisons involving the connectivity matrices assigned to meta-band 1 show statistically significant differences between HC and MCI patients as well. Additionally, when comparing the connectivity matrices assigned to meta-band 2 and the network topologies of meta-bands 2 and 3, statistically significant differences between patients with MCI and AD can also be observed.

The differences in the mean and standard deviation of the AS are depicted in Fig. 4. The mean of the AS shows a decrease with the development of the pathology, with statistically significant differences between HC and AD patients. On the other hand, the standard deviation of the AS seems to be less affected by the pathology, with no statistically significant differences between groups. It is noteworthy that the data distribution of the HC_{train} group shows a distribution of values closer to the HC_{test} than to the other groups, specially for the AS.

In Fig. 4, the data distribution of the mean and standard deviation of the DoD across groups can be appreciated. Both metrics, the mean and the standard deviation of the DoD, show a similar tendency: values become smaller along with the development of the dementia. Furthermore, while the mean of the DoD shows statistically significant differences between HC and AD patients, the standard deviation of the DoD obtains statistically significant differences for the three comparisons under study (HC-MCI, HC-AD, and MCI-AD). As expected, DoD values for HC_{train} are closer to those for HC_{test} than for the pathological groups.

3.4. Alterations in the meta-band sequencing

Fig. 5 shows the data distribution for the SR and B_{LZC} for all the groups under study. Despite the aforementioned differences in the patterns that they characterise, both metrics display increasing values with the progression of the pathology. Furthermore, both of them display statistically significant differences between HC and AD patients.

4. Discussion

In this study, we have characterised the frequency-dependent connectivity structure of MEG signals in elderly controls, MCI patients and AD patients, using a distinct subset of healthy controls as a reference group. Our findings demonstrated that: (i) the CMB algorithm is sensitive to the alterations provoked by MCI and AD in the underlying meta-band structure; (ii) the novel metrics introduced in this study are useful to quantify subtle changes in frequency-dependent connectivity structure.

4.1. The frequency-dependent functional connectivity patterns

Firstly, it is noteworthy that the meta-band segmentation presented in this study exhibits considerable deviation from conventional frequency band segmentations. The CMB methodology proposes an alternative, automatic, FC-based, and subject-specific frequency band segmentation that shifts the focus of the conventional approaches. Thus, the observed differences in the results between the two approaches are reasonable. However, it is still possible to find common points between them, such as the identification of a meta-band around the canonical alpha band. For a more comprehensive comparison of the CMB

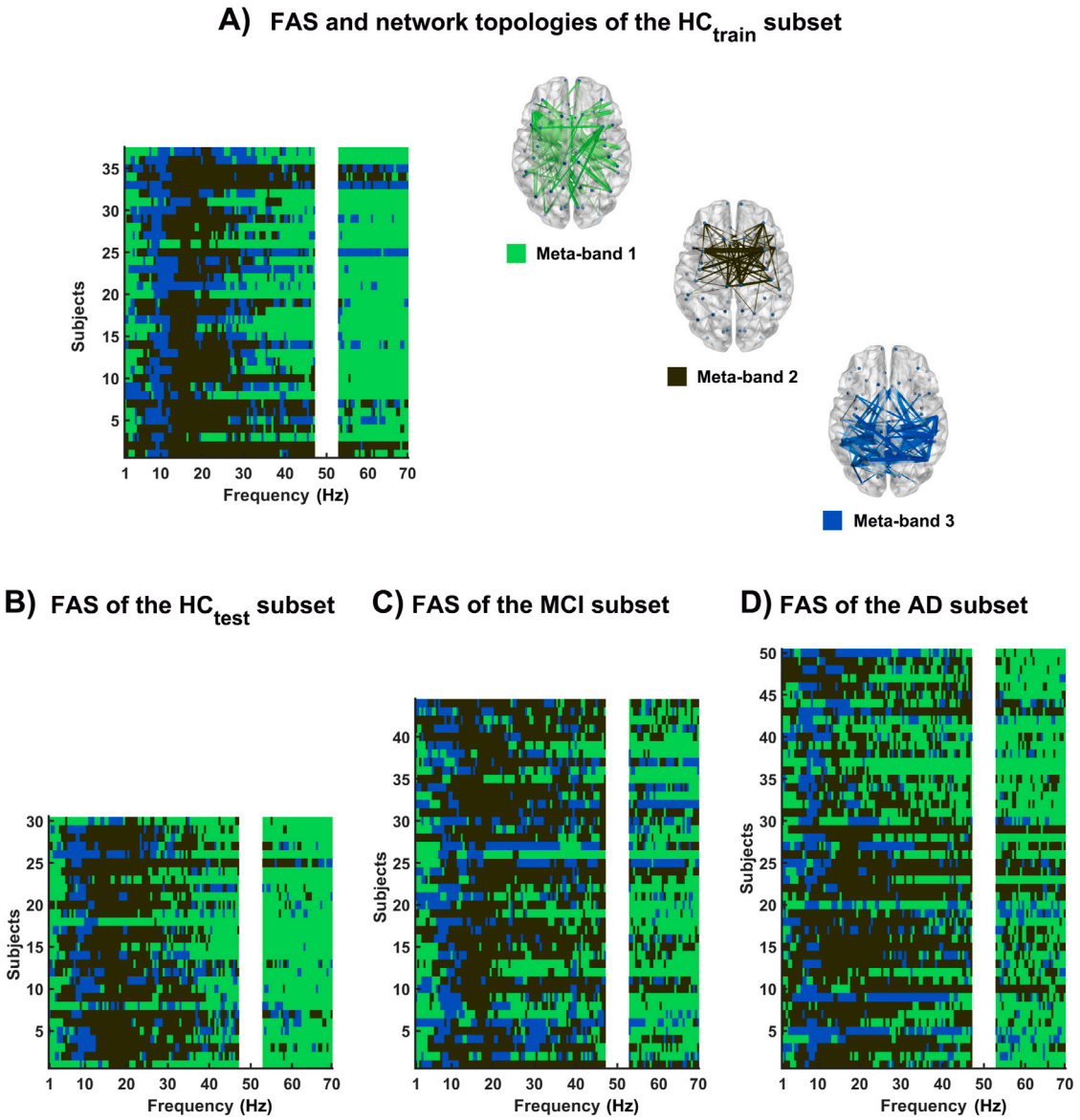

Fig. 2. (A) FAS and network topology of the three main meta-bands detected for the reference (*i.e.*, HC_{train}) group. (B) FAS of each subject of the HC_{test} subset, extracted using the reference (HC_{train}) network topologies. (C) FAS of each subject of the MCI group, extracted using the reference (HC_{train}) network topologies. (D) FAS of each subject of the AD group, extracted using the reference (HC_{train}) network topologies. Colours in plots indicate the dominant meta-band at each frequency bin (green: meta-band 1; brown: meta-band 2; and blue: meta-band 3).

algorithm with canonical frequency bands, please refer to Rodríguez-González et al. [8]. Furthermore, the identification of non-adjacent meta-bands (*i.e.*, meta-bands expanding across non-adjacent frequency ranges) also deserves further attention. As discussed in [8], several explanations may account for this observation. Firstly, it could be a spurious effect arising from averaging different trials, as it neglects the dynamic behaviour of functional connectivity [22,24]. Secondly, it could be due to cross-frequency coupling patterns, which have been proven to play a pivotal role in resting-state activity [47,48]. Finally, it could be the result of grouping frequencies based on their underlying network topology. Consequently, this does not imply the existence of only three global meta-bands, but rather indicates similar network topologies operating across distant frequencies. For a more detailed explanation of the reasoning behind the non-adjacent meta-bands, please see [8].

The structure of the meta-bands obtained for the HC_{train} subset is consistent with that of a prior study [8]. In that study, 3 meta-bands were identified with a larger sample (123 subjects) that included not only elderly subjects, but also cognitively healthy young volunteers. Thereby, the FAS obtained for the HC subsets (HC_{train} and HC_{test}) is aligned with the outcomes reported by Rodríguez-González et al. [8], where a similar meta-band sequencing was obtained for MEG activity. The most noticeable distinction between the FAS obtained in these studies is evident in the meta-band centred around the alpha band. While this meta-band (*i.e.*, meta-band 3) is predominantly concentrated around alpha frequencies in this study, it exhibited a more significant presence around high beta frequencies in [8]. Two primary factors may account for this discrepancy. Firstly, the difference in sample size, which has been demonstrated to influence the results [8]. Secondly, the differences in age between the samples may also, at least partially,

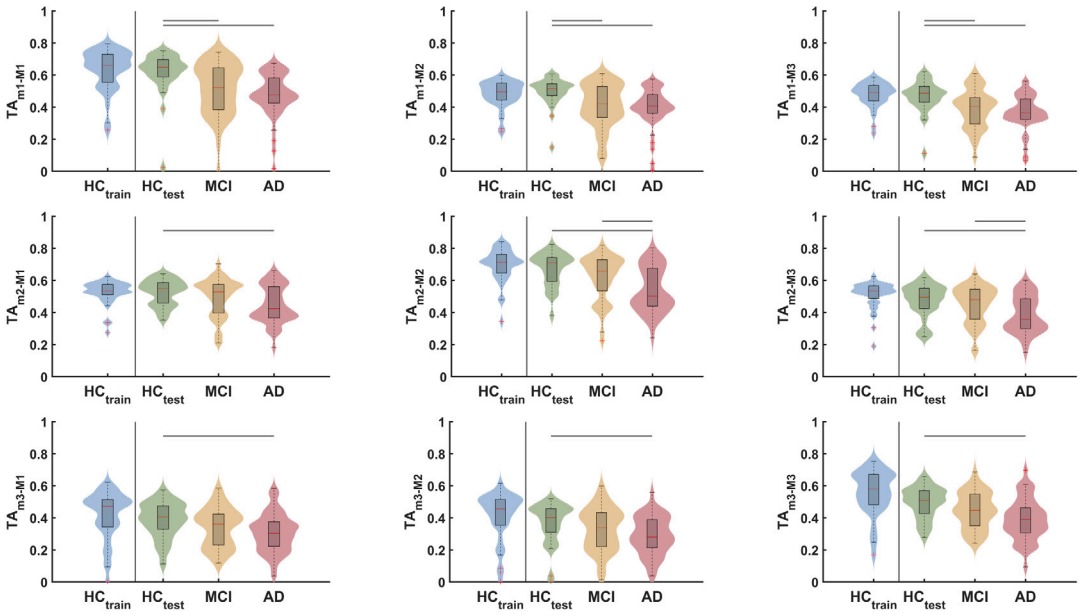

Fig. 3. Distribution plots of the TA between the connectivity matrices assigned to a specific meta-band (rows) and the network topology of the three different meta-bands (columns). Statistically significant between-group differences are indicated with horizontal grey lines ($p < 0.05$, bootstraping approach FDR-corrected). m: mean of the connectivity matrices assigned to a specific meta-band; M: network topology of a specific meta-band; HC_{train}: healthy elderly control train subset (blue); HC_{test}: healthy elderly control test subset (green); MCI: patients with mild cognitive impairment group (yellow); AD: patients with dementia due to Alzheimer's disease group (red). The data distribution of the HC_{train} is displayed for completeness, but it is not included in the comparisons.

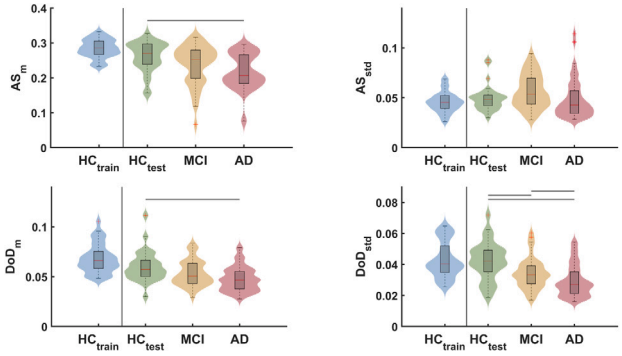

Fig. 4. Distribution plot of the mean (first column), and standard deviation (second column) of the AS (first row) and DoD (second row). Statistically significant between-group differences are indicated with horizontal grey lines ($p < 0.05$, bootstraping approach FDR-corrected). AS: Attraction Strength; DoD: Degree of Dominance, m: mean; std: standard deviation; HC_{train}: healthy elderly control train subset (blue); HC_{test}: healthy elderly control test subset (green); MCI: patients with mild cognitive impairment group (yellow); AD: patients with dementia due to Alzheimer's disease group (red). The data distribution of the HC_{train} is displayed for completeness, but it is not included in the comparisons.

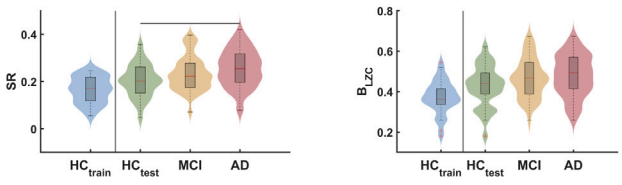

Fig. 5. Distribution plots of the SR and the B_{LZC}. Statistically significant between-group differences are indicated with horizontal grey lines ($p < 0.05$, bootstraping approach FDR-corrected). SR: Structural Richness; B_{LZC}: Band Complexity; HC_{train}: healthy elderly control train group (blue); HC_{test}: healthy elderly control test group (green); MCI: patients with mild cognitive impairment group (yellow); AD: patients with dementia due to Alzheimer's disease group (red). The data distribution of the HC_{train} is displayed for completeness, but it is not included in the comparisons.

contribute to this discrepancy, as it has been established that age can affect functional connectivity patterns [49–51].

4.2. Beyond the disconnection syndrome: blurring of the meta-band structure

This study provides novel evidence that the structure of the meta-bands is progressively altered by dementia, as indicated by TA, AS, and DoD metrics. Previous research has identified alterations in functional connectivity patterns associated with MCI and AD, leading to their classification as a disconnection syndromes [19,52–56]. Interestingly, a recent study proposed a novel method that combines deep learning and explainable artificial intelligence to study the frequency-dependent connectivity alterations associated with AD and MCI [57]. This paper focuses on identifying the neural dynamics that reflect the transition between these two pathological states [57]. However, the current work is the first study to consider these alterations as a dilution of the underlying frequency structure, rather than solely a disconnection.

The findings of the current study suggest that dementia alters the frequency-dependent structure of connectivity, as demonstrated by the TA metric, which showed statistically significant differences between HC and AD groups. This result is consistent with previous studies by Knyazeva and colleagues [58,59], who observed global functional connectivity alterations in AD when analysing the broadband. Additionally, the connectivity matrices assigned to the meta-band 1 showed significant differences between HC and MCI patients across all comparisons. Given that these matrices appear around delta and gamma frequencies, the results suggest that early alterations associated with dementia may manifest in these frequency bands. This is consistent with previous studies that have reported alterations in functional connectivity in MCI and early AD patients in delta [60–62] and gamma frequencies [63]. Interestingly, delta and theta functional connectivity have been found to be associated with the progression from MCI to AD [62]. In the same study, it can be appreciated that the differences in functional connectivity between HC and MCI are not produced in specific brain regions but in a widespread fashion [62]. This is in line with the topology of the connectivity matrices assigned to the meta-band 1; although this should be carefully interpreted as the comparison is not

straightforward. Additionally, the comparisons between the connectivity matrices assigned to the meta-band 2 and the meta-bands 2 and 3, display statistically significant differences between HC and AD patients, and between MCI patients and AD patients (but not between HC and MCI patients). These matrices correspond with frequency bins around the conventional beta band, having a mid-frontal network topology, which suggests that the pathological alterations in these frequencies and brain areas have not yet emerged in the MCI phase.

The AS displays only statistically significant values in the comparison between HC and AD patients. This indicates that the adaptation of the connectivity matrices to the dominant meta-band is only affected in later stages of the pathology. Meanwhile, the DoD metric shows statistically significant differences in mean values between HC and AD patients, and in standard deviation values for all three comparisons (HC-AD, HC-MCI, and MCI-AD). These findings suggest that the pathological changes not only reduce the adaptation of the connectivity matrices to the dominant meta-band, but also the similarity balance between the dominant meta-band and other meta-bands, likely to a greater extent, resulting in a decreased similarity balance. These findings point out to a dilution of the network topologies in pathological states, compared to those of the HC subjects, as: (i) the similarity with the dominant meta-band is decreased; (ii) the difference in similarity between the dominant meta-band and the other ones is decreased; (iii) the standard deviation of the previous metric (DoD) is also reduced. These pathological alterations result in more homogeneous topologies, suggesting the loss of specialised and integrated networks, with their functions assumed by other brain regions. This is in line with previous studies that have used EEG and MEG signals to demonstrate that AD patients exhibit decreased clustering coefficient and modularity, indicative of more heterogeneous and widespread network topologies [64–66]

SR and B_{LZC} display a similar pattern, with progressively increasing values for MCI and AD patients and statistically significant differences between HC and AD patients. Nonetheless, as it has been previously stated, they reflect different properties of the meta-band structure. Firstly, the results obtained with SR indicate that MCI and AD can be associated with less stable meta-bands. This metric is similar to the dwell time used in a previous study by Núñez and colleagues, which characterised the stability of time-dependent meta-states [22]. In that study, it was observed that the stability of the meta-states decreased for MCI and AD patients, which is in agreement with our findings [22]. It is worth noting that a previous study reported a decreased transition frequency for AD patients, which is related to the width of the alpha band [67]. This narrowing of the alpha band may be a consequence of the disruption of the frequency-dependent connectivity structure that we observed in MCI and AD patients. As suggested by Moretti and colleagues, these alterations might be associated with compensatory mechanisms [67]. Moreover, the dilution of the meta-band structure observed in the pathological patients results in an increased number of meta-band changes. In this regard, we also observed an increase in B_{LZC} for pathological patients, which suggests that the mechanisms governing meta-band transitions are affected by the disease. Notably, a previous study reported an increase in the complexity of time-dependent EEG meta-state sequencing [22]. Both findings support the notion of a gradual loss of the time-frequency structure of the functional neural network associated with AD progression. Regarding temporal meta-states, it has been observed that more stable meta-states are a way to keep the efficiency of the networks [68, 69]. Furthermore, the efficiency of temporal meta-state transitions has been linked to higher cognitive functions [69]. Hence, the decreased complexity of the FAS for HC may be attributed to an optimisation of brain function, where the number of transitions between meta-bands is limited.

This study applies a novel algorithm to evaluate the alterations that MCI and AD elicit in MEG signals. It employs a completely new perspective, laying the groundwork for further investigations. Our findings demonstrate that distinct frequency-dependent connectivity patterns are present during rest among HC, MCI, and AD patients. These findings are of utmost significance, as they shed light on the underlying mechanisms of AD progression and offer a potential explanation for the lack of consensus in network dynamics observed in this disease [70–72].

4.3. Limitations and future lines

Although this study has yielded very interesting and promising results, there are some limitations that should be further considered. First, the CMB methodology itself present some constraints (*i.e.*, it has been optimised for resting-state signals; it requires to select some hyperparameters; and it considers the FC stable in time). A more detailed description of the CMB methodology can be found in [8]. This algorithm, employs the Louvain GJA community detection methodology as it does not require to *a-priori* define the number of communities to be detected. Nonetheless, it could be interesting to explore the results using other community detection methods, such as Infomap or Newman's Spectral Approach, to verify the consistency of the findings [73].

Furthermore, a per-group community detection approach was employed, enabling direct comparisons of detected meta-bands across groups. However, the use of an individual (*i.e.*, subject-based) community detection approach would emphasise individual differences. Future studies could consider utilising this approach in conjunction with longitudinal neurophysiological recordings, which may uncover subject-specific alterations related to the trajectory of AD. Also, it could be useful to not only consider the FAS, which is a "hard" assignment of the dominant meta-band in each frequency bin, but also use the specific correlation values with each of the detected meta-bands [24].

Finally, the performance of the CMB methodology has been previously assessed in EEG recordings (with 19 and 32 channels), demonstrating a decreased performance compared to MEG signals [8]. The CMB methodology should also be tested with other neuroimaging techniques (*e.g.*, fMRI or high-density EEG), to further evaluate the robustness of the results across different modalities of functional brain imaging.

5. Conclusions

In this study, we have applied a novel methodology to identify the alterations in the frequency-dependent connectivity structure of resting-state MEG recordings induced by MCI and AD. Our analysis has revealed a gradual blurring of network topologies associated with AD progression, as indicated by the TA, DoD, and AS metrics. Furthermore, SR and B_{LZC} metrics indicate that the meta-band sequencing is also diluted, with a more complex and heterogeneous frequency-dependent structure in MCI and AD patients. The metrics that we have proposed here are capable of quantifying the subtle alterations that MCI and AD elicit in the frequency-dependent structure of neural signals, and may be used in future studies to facilitate the diagnosis of MCI and AD.

CRediT authorship contribution statement

Víctor Rodríguez-González: Conceptualization, Methodology, Software, Formal analysis, Investigation, Writing – original draft, Visualization, Data curation. **Pablo Núñez:** Methodology, Software, Formal analysis, Writing – review & editing. **Carlos Gómez:** Conceptualization, Methodology, Data curation, Writing – review & editing, Visualization, Supervision. **Hideyuki Hoshi:** Resources, Data curation, Writing – review & editing. **Yoshihito Shigihara:** Resources, Data curation, Writing – review & editing. **Roberto Hornero:** Conceptualization, Writing – review & editing, Supervision, Funding acquisition. **Jesús Poza:** Conceptualization, Methodology, Data curation, Writing – review & editing, Visualization, Supervision, Funding acquisition.

Declaration of competing interest

The authors declare the following financial interests/personal relationships which may be considered as potential competing interests: Hideyuki Hoshi reports financial support was provided by Ricoh Company Limited.

Data availability

Data will be made available on request.

Acknowledgements

This research has been funded by 'CIBER en Bioingeniería, Biomateriales y Nanomedicina (CIBER-BBN)' through 'Instituto de Salud Carlos III' co-funded with ERDF funds. Vítor Rodríguez-González was in receipt of a PIF-UVa grant from the 'University of Valladolid' and a 'Movilidad Doctorandos y Doctorandas UVa 2022' grant. P. Núñez was funded by the ERA-Net FLAG-ERA JTC2021 project ModelDXConsciousness (Human Brain Project Partnering Project).

Appendix A. Supplementary data

Supplementary material related to this article can be found online at https://doi.org/10.1016/j.bspc.2023.105512.

References

[1] A. Association, 2022 Alzheimer's disease facts and figures, Alzheimer's Dement. 18 (4) (2022) 700–789, http://dx.doi.org/10.1002/alz.12638.

[2] C. Babiloni, V. Pizzella, C.D. Gratta, A. Ferretti, G.L. Romani, Fundamentals of electroencefalography, magnetoencefalography, and functional magnetic resonance imaging, Int. Rev. Neurobiol. 86 (2009) 67–80, http://dx.doi.org/10.1016/S0074-7742(09)86005-4.

[3] G. Deco, V.K. Jirsa, A.R. McIntosh, Resting brains never rest: computational insights into potential cognitive architectures, Trends Neurosci. 36 (2013) 268–274, http://dx.doi.org/10.1016/j.tins.2013.03.001.

[4] L. Waschke, N.A. Kloosterman, J. Obleser, D.D. Garrett, Behavior needs neural variability, Neuron 109 (2021) 751–766, http://dx.doi.org/10.1016/j.neuron.2021.01.023.

[5] S. Singh, Magnetoencephalography: Basic principles, Ann. Indian Acad. Neurol. 17 (2014) 107, http://dx.doi.org/10.4103/0972-2327.128676.

[6] M. Illman, K. Laaksonen, M. Liljeström, V. Jousmäki, H. Piitulainen, N. Forss, Comparing MEG and EEG in detecting the 20-Hz rhythm modulation to tactile and proprioceptive stimulation, NeuroImage 215 (2020) 116804, http://dx.doi.org/10.1016/j.neuroimage.2020.116804.

[7] S. Supek, C.J. Aine (Eds.), Magnetoencephalography, second ed., Springer International Publishing, Cham, Switzerland, 2019, p. 1358, http://dx.doi.org/10.1007/978-3-030-00087-5.

[8] V. Rodríguez-González, P. Núñez, C. Gómez, Y. Shigihara, H. Hoshi, M.Á. Tola-Arribas, M. Cano, Á. Guerrero, D. García-Azorín, R. Hornero, J. Poza, Connectivity-based Meta-Bands: A new approach for automatic frequency band identification in connectivity analyses, NeuroImage 280 (120332) (2023) 1–18, http://dx.doi.org/10.1016/j.neuroimage.2023.120332.

[9] P.K. Mandal, A. Banerjee, M. Tripathi, A. Sharma, A comprehensive review of magnetoencephalography (MEG) studies for brain functionality in healthy aging and Alzheimer's Disease (AD), Front. Comput. Neurosci. 12 (2018) http://dx.doi.org/10.3389/fncom.2018.00060.

[10] M. Engels, W. van der Flier, C. Stam, A. Hillebrand, P. Scheltens, E. van Straaten, Alzheimer's disease: The state of the art in resting-state magnetoencephalography, Clin. Neurophysiol. 128 (2017) 1426–1437, http://dx.doi.org/10.1016/j.clinph.2017.05.012.

[11] D. López-Sanz, N. Serrano, F. Maestú, The role of magnetoencephalography in the early stages of Alzheimer's disease, Front. Neurosci. 12 (2018) http://dx.doi.org/10.3389/fnins.2018.00572.

[12] J. Sun, B. Wang, Y. Niu, Y. Tan, C. Fan, N. Zhang, J. Xue, J. Wei, J. Xiang, Complexity analysis of EEG, MEG, and fMRI in mild cognitive impairment and alzheimer's disease: A review, Entropy 22 (2020) 239, http://dx.doi.org/10.3390/e22020239.

[13] C.J. Stam, E.C.W. van Straaten, The organization of physiological brain networks, Clin. Neurophysiol. 123 (2012) 1067–1087, http://dx.doi.org/10.1016/j.clinph.2012.01.011.

[14] J. Dauwels, K. Srinivasan, M.R. Reddy, T. Musha, F.-B. Vialatte, C. Latchoumane, J. Jeong, A. Cichocki, Slowing and loss of complexity in Alzheimer's EEG: Two sides of the same coin? Int. J. Alzheimer's Dis. 2011 (2011) 1–10, http://dx.doi.org/10.4061/2011/539621.

[15] C. Gómez, R. Hornero, Entropy and complexity analyses in Alzheimer's Disease: An MEG study, Open Biomed. Eng. J. 4 (2010) 223–235, http://dx.doi.org/10.2174/1874120701004010223.

[16] S.J. Ruiz-Gómez, C. Gómez, J. Poza, M. Martínez-Zarzuela, M.A. Tola-Arribas, M. Cano, R. Hornero, Measuring alterations of spontaneous EEG neural coupling in Alzheimer's disease and mild cognitive impairment by means of cross-entropy metrics, Front. Neuroinform. 12 (2018) 1–11, http://dx.doi.org/10.3389/fninf.2018.00076.

[17] G.T. Vallet, C. Hudon, M. Simard, R. Versace, The disconnection syndrome in the Alzheimer's disease: The cross-modal priming example, Cortex 49 (2013) 2402–2415, http://dx.doi.org/10.1016/j.cortex.2012.10.010.

[18] X. Delbeuck, M.V.D. Linden, F. Collette, Alzheimer's disease as a disconnection syndrome? Neuropsychol. Rev. 13 (2003).

[19] X. Delbeuck, F. Collette, M.V. der Linden, Is Alzheimer's disease a disconnection syndrome? Neuropsychologia 45 (2007) 3315–3323, http://dx.doi.org/10.1016/j.neuropsychologia.2007.05.001.

[20] J. Schumacher, L.R. Peraza, M. Firbank, A.J. Thomas, M. Kaiser, P. Gallagher, J.T. O'Brien, A.M. Blamire, J.-P. Taylor, Dynamic functional connectivity changes in dementia with Lewy bodies and Alzheimer's disease, NeuroImage: Clin. 22 (2019) 101812, http://dx.doi.org/10.1016/j.nicl.2019.101812.

[21] P.N. nez, J. Poza, C. Gómez, V. Rodríguez-González, A. Hillebrand, M.A. Tola-Arribas, M. Cano, R. Hornero, Characterizing the fluctuations of dynamic resting-state electrophysiological functional connectivity: reduced neuronal coupling variability in mild cognitive impairment and dementia due to Alzheimer's disease, J. Neural Eng. 16 (2019) 056030, http://dx.doi.org/10.1088/1741-2552/ab234b.

[22] P.N. nez, J. Poza, C. Gómez, V. Rodríguez-González, A. Hillebrand, P. Tewarie, M.Á. Tola-Arribas, M. Cano, R. Hornero, Abnormal meta-state activation of dynamic brain networks across the alzheimer spectrum, NeuroImage 232 (2021) 117898, http://dx.doi.org/10.1016/j.neuroimage.2021.117898.

[23] Y. Gu, Y. Lin, L. Huang, J. Ma, J. Zhang, Y. Xiao, Z. Dai, Abnormal dynamic functional connectivity in Alzheimer's disease, CNS Neurosci. Ther. 26 (2020) 962–971, http://dx.doi.org/10.1111/cns.13387.

[24] P.N. nez, C. Gómez, V. Rodríguez-González, A. Hillebrand, P. Tewarie, J. Gomez-Pilar, V. Molina, R. Hornero, J. Poza, Schizophrenia induces abnormal frequency-dependent patterns of dynamic brain network reconfiguration during an auditory oddball task, J. Neural Eng. 19 (2022) 016033, http://dx.doi.org/10.1088/1741-2552/ac514e.

[25] J.J. Newson, T.C. Thiagarajan, EEG frequency bands in psychiatric disorders: A review of resting state studies, Front. Hum. Neurosci. 12 (2019) 1–24, http://dx.doi.org/10.3389/fnhum.2018.00521.

[26] P. Núñez, J. Poza, C. Gómez, V. Barroso-García, A. Maturana-Candelas, M.A. Tola-Arribas, M. Cano, R. Hornero, Characterization of the dynamic behavior of neural activity in Alzheimer's disease: exploring the non-stationarity and recurrence structure of EEG resting-state activity, J. Neural Eng. 17 (1) (2020) 016071, http://dx.doi.org/10.1088/1741-2552/ab71e9.

[27] M.S. Albert, S.T. DeKosky, D. Dickson, B. Dubois, H.H. Feldman, N.C. Fox, A. Gamst, D.M. Holtzman, W.J. Jagust, R.C. Petersen, P.J. Snyder, M.C. Carrillo, B. Thies, C.H. Phelps, The diagnosis of mild cognitive impairment due to Alzheimer's disease: Recommendations from the National Institute on Aging-Alzheimer's Association workgroups on diagnostic guidelines for alzheimer's disease, Alzheimer's Dement. 7 (2011) 270–279, http://dx.doi.org/10.1016/j.jalz.2011.03.008.

[28] G.M. McKhann, D.S. Knopman, H. Chertkow, B.T. Hyman, C.R. Jack, C.H. Kawas, W.E. Klunk, W.J. Koroshetz, J.J. Manly, R. Mayeux, R.C. Mohs, J.C. Morris, M.N. Rossor, P. Scheltens, M.C. Carrillo, B. Thies, S. Weintraub, C.H. Phelps, The diagnosis of dementia due to alzheimer's disease: Recommendations from the national institute on aging-alzheimer's association workgroups on diagnostic guidelines for Alzheimer's disease, Alzheimer's Dement. 7 (2011) 263–269, http://dx.doi.org/10.1016/j.jalz.2011.03.005.

[29] V. Rodríguez-González, C. Gómez, Y. Shigihara, H. Hoshi, M. Revilla-Vallejo, R. Hornero, J. Poza, Consistency of local activation parameters at sensor- and source-level in neural signals, J. Neural Eng. 17 (2020) 056020, http://dx.doi.org/10.1088/1741-2552/abb582.

[30] T.P. Mutanen, J. Metsomaa, S. Liljander, R.J. Ilmoniemi, Automatic and robust noise suppression in EEG and MEG: The SOUND algorithm, NeuroImage 166 (2018) 135–151, http://dx.doi.org/10.1016/j.neuroimage.2017.10.021.

[31] F.-H. Lin, T. Witzel, M.S. Hämäläinen, A.M. Dale, J.W. Belliveau, S.M. Stufflebeam, Spectral spatiotemporal imaging of cortical oscillations and interactions in the human brain, NeuroImage 23 (2004) 582–595, http://dx.doi.org/10.1016/j.neuroimage.2004.04.027.

[32] L. Tait, A. Özkan, M.J. Szul, J. Zhang, A systematic evaluation of source reconstruction of resting MEG of the human brain with a new high-resolution atlas: Performance, precision, and parcellation, Hum. Brain Mapp. 42 (2021) 4685–4707, http://dx.doi.org/10.1002/hbm.25578.

[33] J. Rizkallah, H. Amoud, M. Fraschini, F. Wendling, M. Hassan, Exploring the correlation between M/EEG source–space and fMRI networks at rest, Brain Topogr. 33 (2020) 151–160, http://dx.doi.org/10.1007/s10548-020-00753-w.
[34] L. Larson-Prior, R. Oostenveld, S.D. Penna, G. Michalareas, F. Prior, A. Babajani-Feremi, J.-M. Schoffelen, L. Marzetti, F. de Pasquale, F.D. Pompeo, J. Stout, M. Woolrich, Q. Luo, R. Bucholz, P. Fries, V. Pizzella, G. Romani, M. Corbetta, A. Snyder, Adding dynamics to the Human Connectome Project with MEG, NeuroImage 80 (2013) 190–201, http://dx.doi.org/10.1016/j.neuroimage.2013.05.056.
[35] F. Tadel, S. Baillet, J.C. Mosher, D. Pantazis, R.M. Leahy, Brainstorm: A user-friendly application for MEG/EEG analysis, Comput. Intell. Neurosci. 2011 (2011) 1–13, http://dx.doi.org/10.1155/2011/879716.
[36] V.S. Fonov, A.C. Evans, R.C. McKinstry, C.R. Almli, D.L. Collins, Unbiased nonlinear average age-appropriate brain templates from birth to adulthood, NeuroImage 47 (2009) S102, http://dx.doi.org/10.1016/S1053-8119(09)70884-5.
[37] L. Douw, D. Nieboer, C.J. Stam, P. Tewarie, A. Hillebrand, Consistency of magnetoencephalographic functional connectivity and network reconstruction using a template versus native MRI for co-registration, Hum. Brain Mapp. 39 (2018) 104–119, http://dx.doi.org/10.1002/hbm.23827.
[38] A. Gramfort, T. Papadopoulo, E. Olivi, M. Clerc, OpenMEEG: opensource software for quasistatic bioelectromagnetics, BioMed. Eng. OnLine 9 (2010) 45, http://dx.doi.org/10.1186/1475-925X-9-45.
[39] D. Vidaurre, A.J. Quinn, A.P. Baker, D. Dupret, A. Tejero-Cantero, M.W. Woolrich, Spectrally resolved fast transient brain states in electrophysiological data, NeuroImage 126 (2016) 81–95, http://dx.doi.org/10.1016/j.neuroimage.2015.11.047.
[40] M. Lai, M. Demuru, A. Hillebrand, M. Fraschini, A comparison between scalp- and source-reconstructed EEG networks, Sci. Rep. 8 (2018) 12269, http://dx.doi.org/10.1038/s41598-018-30869-w.
[41] R.S. Desikan, F. Ségonne, B. Fischl, B.T. Quinn, B.C. Dickerson, D. Blacker, R.L. Buckner, A.M. Dale, R.P. Maguire, B.T. Hyman, M.S. Albert, R.J. Killiany, An automated labeling system for subdividing the human cerebral cortex on MRI scans into gyral based regions of interest, NeuroImage 31 (2006) 968–980, http://dx.doi.org/10.1016/j.neuroimage.2006.01.021.
[42] V. Rodriguez-Gonzalez, V.G. de Pablo, C. Gómez, Y. Shigihara, H. Hoshi, R. Hornero, M.Á. Tola-Arribas, M. Cano, J. Poza, High frequential resolution networks: Considerations on a new functional brain connectivity framework, in: 43rd Annual International Conference of the IEEE Engineering in Medicine and Biology Society (EMBC), IEEE, 2021, pp. 722–725.
[43] A. Lempel, J. Ziv, On the complexity of finite sequences, IEEE Trans. Inform. Theory 22 (1976) 75–81, http://dx.doi.org/10.1109/TIT.1976.1055501.
[44] G.A. Rousselet, C.R. Pernet, R.R. Wilcox, The percentile bootstrap: A primer with step-by-step instructions in r, Adv. Methods Pract. Psychol. Sci. 4 (2021) 251524592091188, http://dx.doi.org/10.1177/2515245920911881.
[45] R. Haraguchi, H. Hoshi, S. Ichikawa, M. Hanyu, K. Nakamura, K. Fukasawa, J. Poza, V. Rodríguez-González, C. Gómez, Y. Shigihara, The menstrual cycle alters resting-state cortical activity: A magnetoencephalography study, Front. Hum. Neurosci. 15 (2021) http://dx.doi.org/10.3389/fnhum.2021.652789.
[46] Y. Benjamini, Y. Hochberg, Controlling the false discovery rate: A practical and powerful approach to multiple testing, J. R. Stat. Soc. Ser. B Stat. Methodol. 57 (1995) 289–300, http://dx.doi.org/10.1111/j.2517-6161.1995.tb02031.x.
[47] E. Florin, S. Baillet, The brain's resting-state activity is shaped by synchronized cross-frequency coupling of neural oscillations, NeuroImage 111 (2015) 26–35, http://dx.doi.org/10.1016/j.neuroimage.2015.01.054.
[48] T. Stankovski, V. Ticcinelli, P.V.E. McClintock, A. Stefanovska, Neural cross-frequency coupling functions, Front. Syst. Neurosci. 11 (2017) http://dx.doi.org/10.3389/fnsys.2017.00033.
[49] C.B. Schäfer, B.R. Morgan, A.X. Ye, M.J. Taylor, S.M. Doesburg, Oscillations, networks, and their development: MEG connectivity changes with age, Hum. Brain Mapp. 35 (2014) 5249–5261, http://dx.doi.org/10.1002/hbm.22547.
[50] D.J.A. Smit, M. Boersma, H.G. Schnack, S. Micheloyannis, D.I. Boomsma, H.E.H. Pol, C.J. Stam, E.J.C. de Geus, The brain matures with stronger functional connectivity and decreased randomness of its network, PLoS One 7 (2012) e36896, http://dx.doi.org/10.1371/journal.pone.0036896.
[51] X. Wen, H. He, L. Dong, J. Chen, J. Yang, H. Guo, C. Luo, D. Yao, Alterations of local functional connectivity in lifespan: A resting-state fMRI study, Brain Behav. 10 (2020) http://dx.doi.org/10.1002/brb3.1652.
[52] A. Badhwar, A. Tam, C. Dansereau, P. Orban, F. Hoffstaedter, P. Bellec, Resting-state network dysfunction in Alzheimer's disease: A systematic review and meta-analysis, Alzheimer's Dement.: Diagn. Assess. Dis. Monit. 8 (2017) 73–85, http://dx.doi.org/10.1016/j.dadm.2017.03.007.
[53] R. Ishii, L. Canuet, Y. Aoki, M. Hata, M. Iwase, S. Ikeda, K. Nishida, M. Ikeda, Healthy and pathological brain aging: From the perspective of oscillations, functional connectivity, and signal complexity, Neuropsychobiology 75 (2017) 151–161, http://dx.doi.org/10.1159/000486870.
[54] M.M. Engels, C.J. Stam, W.M. van der Flier, P. Scheltens, H. de Waal, E.C. van Straaten, Declining functional connectivity and changing hub locations in Alzheimer's disease: an EEG study, BMC Neurol. 15 (2015) 145, http://dx.doi.org/10.1186/s12883-015-0400-7.
[55] Y.I. Sheline, M.E. Raichle, Resting state functional connectivity in preclinical Alzheimer's disease, Biol. Psychiat. 74 (2013) 340–347, http://dx.doi.org/10.1016/j.biopsych.2012.11.028.
[56] L. Koelewijn, A. Bompas, A. Tales, M.J. Brookes, S.D. Muthukumaraswamy, A. Bayer, K.D. Singh, Alzheimer's disease disrupts alpha and beta-band resting-state oscillatory network connectivity, Clin. Neurophysiol. 128 (11) (2017) 2347–2357, http://dx.doi.org/10.1016/j.clinph.2017.04.018.
[57] F.C. Morabito, C. Ieracitano, N. Mammone, An explainable Artificial Intelligence approach to study MCI to AD conversion via HD-EEG processing, Clin. EEG Neurosci. 54 (1) (2023) 51–60, http://dx.doi.org/10.1177/15500594211063662.
[58] M.G. Knyazeva, M. Jalili, A. Brioschi, I. Bourquin, E. Fornari, M. Hasler, R. Meuli, P. Maeder, J. Ghika, Topography of EEG multivariate phase synchronization in early Alzheimer's disease, Neurobiol. Aging 31 (2010) 1132–1144, http://dx.doi.org/10.1016/j.neurobiolaging.2008.07.019.
[59] M.G. Knyazeva, C. Carmeli, A. Khadivi, J. Ghika, R. Meuli, R.S. Frackowiak, Evolution of source EEG synchronization in early Alzheimer's disease, Neurobiol. Aging 34 (2013) 694–705, http://dx.doi.org/10.1016/j.neurobiolaging.2012.07.012.
[60] B. Tóth, B. File, R. Boha, Z. Kardos, Z. Hidasi, Z.A. Gaál, É. Csibri, P. Salacz, C.J. Stam, M. Molnár, EEG network connectivity changes in mild cognitive impairment — Preliminary results, Int. J. Psychophysiol. 92 (2014) 1–7, http://dx.doi.org/10.1016/j.ijpsycho.2014.02.001.
[61] N. Handayani, F. Haryanto, S.N. Khotimah, I. Arif, W.P. Taruno, Coherence and phase synchrony analyses of EEG signals in mild cognitive impairment (MCI): A study of functional brain connectivity, Polish J. Med. Phys. Eng. 24 (2018) 1–9, http://dx.doi.org/10.2478/pjmpe-2018-0001.
[62] C.S. Musaeus, M.S. Nielsen, P. Høgh, Altered low-frequency EEG connectivity in mild cognitive impairment as a sign of clinical progression, J. Alzheimer's Dis. 68 (2019) 947–960, http://dx.doi.org/10.3233/JAD-181081.
[63] C. Gómez, C.J. Stam, R. Hornero, A. Fernández, F. Maestú, Disturbed beta band functional connectivity in patients with mild cognitive impairment: An MEG study, IEEE Trans. Biomed. Eng. 56 (2009) 1683–1690, http://dx.doi.org/10.1109/TBME.2009.2018454.
[64] M.R. Brier, J.B. Thomas, A.M. Fagan, J. Hassenstab, D.M. Holtzman, T.L. Benzinger, J.C. Morris, B.M. Ances, Functional connectivity and graph theory in preclinical Alzheimer's disease, Neurobiol. Aging 35 (2014) 757–768, http://dx.doi.org/10.1016/j.neurobiolaging.2013.10.081.
[65] W. de Haan, Y.A. Pijnenburg, R.L. Strijers, Y. van der Made, W.M. van der Flier, P. Scheltens, C.J. Stam, Functional neural network analysis in frontotemporal dementia and Alzheimer's disease using EEG and graph theory, BMC Neurosci. 10 (2009) 101, http://dx.doi.org/10.1186/1471-2202-10-101.
[66] C.J. Stam, W. de Haan, A. Daffertshofer, B.F. Jones, I. Manshanden, A.M. van Cappellen van Walsum, T. Montez, J.P.A. Verbunt, J.C. de Munck, B.W. van Dijk, H.W. Berendse, P. Scheltens, Graph theoretical analysis of magnetoencephalographic functional connectivity in Alzheimer's disease, Brain 132 (2009) 213–224, http://dx.doi.org/10.1093/brain/awn262.
[67] D.V. Moretti, C. Babiloni, G. Binetti, E. Cassetta, G.D. Forno, F. Ferreric, R. Ferri, B. Lanuzza, C. Miniussi, F. Nobili, G. Rodriguez, S. Salinari, P.M. Rossini, Individual analysis of EEG frequency and band power in mild Alzheimer's disease, Clin. Neurophysiol. 115 (2004) 299–308, http://dx.doi.org/10.1016/S1388-2457(03)00345-6.
[68] A. Zalesky, A. Fornito, L. Cocchi, L.L. Gollo, M. Breakspear, Time-resolved resting-state brain networks, Proc. Natl. Acad. Sci. 111 (2014) 10341–10346, http://dx.doi.org/10.1073/pnas.1400181111.
[69] J.P. Ramirez-Mahaluf, V. Medel, Á. Tepper, L.M. Alliende, J.R. Sato, T. Ossandon, N.A. Crossley, Transitions between human functional brain networks reveal complex, cost-efficient and behaviorally-relevant temporal paths, NeuroImage 219 (2020) 117027, http://dx.doi.org/10.1016/j.neuroimage.2020.117027.
[70] R. Franciotti, N.W. Falasca, D. Arnaldi, F. Famà, C. Babiloni, M. Onofrj, F.M. Nobili, L. Bonanni, Cortical network topology in prodromal and mild dementia due to Alzheimer's Disease: Graph theory applied to resting state EEG, Brain Topogr. 32 (2019) 127–141, http://dx.doi.org/10.1007/S10548-018-0674-3/TABLES/4.
[71] C.T. Briels, C.T. Briels, D.N. Schoonhoven, D.N. Schoonhoven, C.J. Stam, H.D. Waal, P. Scheltens, A.A. Gouw, Reproducibility of EEG functional connectivity in Alzheimer's disease, Alzheimer's Res. Ther. 12 (2020) 1–14, http://dx.doi.org/10.1186/s13195-020-00632-3.
[72] M. Jalili, Functional brain networks: Does the choice of dependency estimator and binarization method matter? Sci. Rep. 6 (2016) 29780, http://dx.doi.org/10.1038/srep29780.
[73] K.M. Gates, T. Henry, D. Steinley, D.A. Fair, A Monte Carlo evaluation of weighted community detection algorithms, Front. Neuroinform. 10 (2016) 1–16, http://dx.doi.org/10.3389/fninf.2016.00045.